International Journal for Modern Trends in Science and Technology
Volume 9, Issue 08, pages 70-79
ISSN: 2455-3778 online
Available online at: http://www.ijmtst.com/vol9issue09.html
DOI: https://doi.org/10.46501/IJMTST0909013

Development of a Multifunctional Non-Isolated Dual Input-Dual Output Converter using Advanced Controller for Electric Vehicle Applications

Siva Prasad .Rathina[1] | Dr. K. Siva Kumar[2]

[1]Department of EEE, Sri Venkatesa Perumal College of Engineering and Technology, Puttur, Andhrapradesh, India
[2]Department of EEE, Sri Venkatesa Perumal College of Engineering and Technology, Puttur, Andhrapradesh, India

To Cite this Article
Siva Prasad .Rathina and Dr. K. Siva Kumar. Development of a Multifunctional Non-Isolated Dual Input-Dual Output Converter using Advanced Controller for Electric Vehicle Applications, 2023, 9(09), pages. 70-79.https://doi.org/10.46501/IJMTST0909013

Article Info
Received: 28 August 2023; Accepted: 20 September 2023; Published: 24 September 2023.

ABSTRACT

High voltage DC/DC converters have gained significant prominence in various power electronics applications in recent years. This is particularly evident in the context of DC microgrids and electric vehicle (EV) systems where multi-port converter structures play a pivotal role. This paper delves into a modified structure of a non-isolated four-port converter, featuring two input and two output ports, tailored for electric vehicle applications. A standout feature of this converter is its capacity to accommodate energy resources with diverse voltage and current characteristics, offering simultaneous buck and boost output capabilities during its operation. The proposed four-port converter (FPC) showcases reduced component count and a simplified control strategy, rendering it a more reliable and cost-effective solution. Additionally, the converter is inherently capable of bidirectional power flow, making it well-suited for recharging the vehicle's battery during regenerative braking. In this paper, we thoroughly analyze the steady-state and dynamic behavior of the converter, presenting a control scheme to efficiently regulate power flow between the various energy sources. Furthermore, we develop a small-signal model to aid in the design of the proposed converter. To validate its design and performance characteristics, extensive MATLAB simulations and experimental tests are conducted under a range of operating conditions. Moreover, to enhance the converter's adaptability and intelligence, an Advanced Controller (ANN) is integrated, enabling real-time optimization of power flow and enhancing its performance in dynamic EV environments. This paper demonstrates the practicality and efficiency of the proposed converter design, highlighting its potential to advance the integration of diverse energy resources within the electric vehicle ecosystem.

KEYWORDS: Multi-port converter, electric vehicle, bidirectional dc/dc converter, artificial neural network, battery storage, regenerative charging.

1. INTRODUCTION

As a result of issues including increasing pollution, exorbitant fuel prices, climate change, and the depletion of fossil fuels, innovative vehicle technologies have arisen as a solution. As a result, manufacturers have shifted their focus to creating environmentally friendly

vehicles like EVs and HEVs. The motor drive system is essential to these vehicles' functionality. An effective power electronic converter is required to power the motor drive system. In order to link renewable energy sources to storage batteries and propulsion motors, power electronic converters used in EVs must be bidirectional. There is a plethora of reports of research efforts in the field of power electronic interfaces for EV systems. In [1], several types of non-isolated three-port converters, such as those made up of a dual input/dual output (DIC/DOC) converter and a single input/single output (SISO) converter, are described. Combining the advantages of the KY converter and the buck-boost converter, the step-up converter shown in [2] achieves a high voltage conversion ratio. A double switch buck-boost converter with interleaving is offered as a method to improve conversion efficiency [3].Non-isolated boost converters with high voltage gains that may self-balance when subjected to an imbalanced load are studied in [4]. Bang and Park [5] detail a buck-cascaded buck-boost power factor correction converter that is suitable for significant input voltage fluctuations. Those converters can only be used in one direction since they are SISO setup. A SISO model of a four-switch, bidirectional dc/dc converter is shown in [6]. In [7], we compare and contrast two forms of bidirectional converters, the cascaded buck-boost capacitor in the centre and the cascaded buck-boost inductor in the middle, to determine their similarities and differences. The authors of [8] propose a zero-voltage-transition, three-level dc/dc converter with soft switching to optimise efficiency and power density. Using three inductors and three active switches, the converter depicted in [9] may provide either buck or boost output, making it a three-port bidirectional design. Power management and control methods for a wide range of parallel buck-boost converter topologies are investigated in detail in [10]. This includes converters that use two modules of supercapacitors. Multi-port energy converters, as seen in [11], employ a single active switching element with many legs to regulate and monitor the output power. More passive components are used in the aforementioned converter than in a regular buck-boost converter. The DC transformer in [12]'s bidirectional high-gain step-up/down dc converter causes the converter to be bulkier than required because of the converter's non-isolated construction. The single-switch buck-boost design shown in [13], [14] is preferable to the challenges observed with the KY converter since it inherits the SISO mode of operation and characteristics of CUK converters. The boost converter, described in [15], [16], is a non-isolated MIMO dc/dc converter that might be used in photovoltaic applications requiring unidirectional power flow. Having just (n-1) stages conduct the buck-boost operation and the nth stage always acting as a boost converter is a drawback of multi-input single-output n-stage converters, as detailed in [17], [18]. The switched capacitor technique, as described in [19], [20], may be implemented in a circuit design that can process multiple inputs. When the number of input sources is equal to the number of active and passive components used, circuit topology and control complexity increase. The non-isolated multi-port converter with a single inductor is suggested for low-power applications in [21], [22]. However, this design requires more than one active switch. Multiport dc/dc converters like the one described in [23] are isolated two-way converters. The larger footprint of the converter is due to the multi-winding transformer that allows for more efficient power transfer. Numerous multiport bidirectional dc/dc converter topologies are possible when dc-link is combined with magnetic coupling [24]. The SISO universal dc/dc converter [25] may be operated in either direction. A dual input dual output converter is recommended [26] for the hybrid electric vehicle. One important problem is that the batteries cannot be used to share the workload. Since [27], you may get a solar-powered electric vehicle that also runs on batteries. To provide for the smooth exchange of power between the EV's battery and solar panels, a dc/dc converter setup is included. The number of switches in this converter is proportional to the number of battery modules; for example, if there are 'n' battery modules, the system will need '2n' switches. To avoid issues like excessive hyper capacitor charging and excessive battery current at peak power, a fuzzy logic control based energy management solution has been proposed [28]. One of the novel ideas given here is a buck-boost converter that operates with just three switches and eliminates the need for a transformer. The suggested converter has many advantages over previously reported topologies (see Table 1), such as its modular design, reduced number of parts, and

adaptability to a wide range of input voltages and currents. Additionally, the proposed converter may "buck" (generate an output voltage lower than the input voltage) or "boost" (generate an output voltage higher than the input voltage). The efficiency of the proposed converter is improved by reducing switching losses to a minimum.

2. Evolution of Multiple Ports in a Buck-Boost Converter

A. Structure of FPC Topology

Because of fluctuations in input power and changing loads in the electric vehicle system, a static power source is insufficient. Consequently, it is crucial to hybridise all current energy sources. In this study, we conceptualise a converter architecture that might connect various energy sources to the gearbox of a moving vehicle. Power electronic interface (a) and its role in the EV's power system (b). The proposed solution employs a four-port converter (FPC), as illustrated in Figure 2. The most notable features of the proposed converter are:

- Bidirectional power flow capability
- Individual power flow control between the sources
- Easy design, control, and implementation process

The three moveable switches Q1, Q2, and Q3 in Figure 2 control the flow of electricity between the load and the input sources. The proposed converter may operate in one of five states, shown in Figures 3a–3e. In the first stage, just one input is used to generate two outputs. As can be seen in Figure 3a, the EV's drive train (the load) is being powered by PV energy in this setup. As can be seen in Figures 3b and 3e, the battery may be charged by either the input PV power or the load in the proposed design. Regenerative braking occurs in state 5 to replenish the battery from the kinetic energy of the load. In the event that the PV is unable to generate enough power due to low irradiation, the battery will drain to provide all of the required energy (see Figure 3c). At times of high demand, the drive train receives power from a battery unit and PV. Once the converter reaches the DIDO state (shown in Figure 3d), processing may begin.

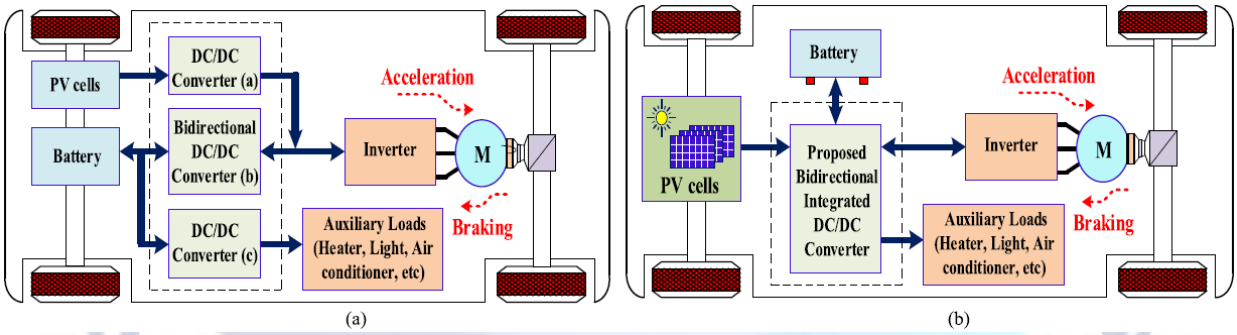

Fig.1 Block diagram of (a) Conventional converter (b) Proposed integrated four-port converter (FPC) interface in an electric vehicle system.

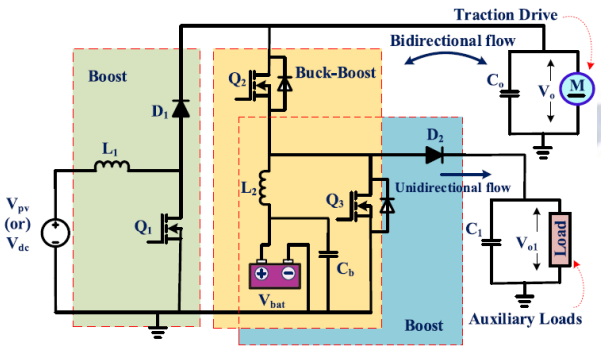

Fig.2 Topology diagram of four-port (FPC) converter.

B. The first operational mode, State 1 SIDO (Single Input Dual Output), has a single input and two outputs. Converter activity (power conversion from PV (Vo, Vo1) to load)

In this case, PV is employed for point-to-load power transfers. Table 2 shows the various machines and their associated switching systems. From zero to d1Ts, switches Q1 and Q3 are active while switches Q2 and Q4 are inoperable. Current via inductor L1 steadily rises whenever a voltage is placed across it that is greater than Vbat. Between d1Ts and Ts, only Q2 is correct, whereas Q1 and Q3 are incorrect. Inductor L1 stores energy for

the previous d1Ts period, and diode D1 transfers that energy to the output capacitor. Ts represents the time elapsed between toggles. The output voltage may be determined under the assumption of a steady state situation as

$$V_0 = \frac{1}{1-d_1} V_{PV} \quad (1)$$

$$V_{01} = \frac{1}{1-d_1} V_{PV} \quad (2)$$

C. This is the Single Input Three Output (State 2) Phase. Converter Condition (PV Energy Transfer to Battery and Load)

This state's functionality is similar to that of state 1. Q2 interacts with d2 0:5 to charge the battery while power is being supplied by PV. Q3 functions similarly to Q1 with d1 > 0:5 to increase output uniformly throughout the load. The equation relates the voltages Vbat, Vpv, Vo, and Vo1.

$$V_0 = \frac{1}{1-d_1} V_{PV} \quad (3)$$

$$V_{01} = d_2 V_{PV} \quad (4)$$

$$V_{bat} = d_2 V_{PV} \quad (5)$$

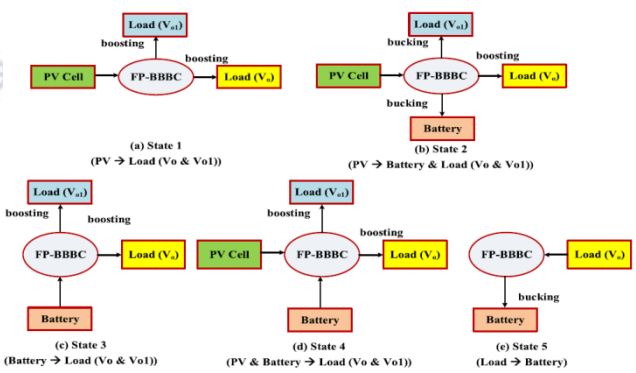

Fig. 3 a) State 1(boost), b) State 2 (buck & boost), c) State 3 (boost), d) State 4 (boost), e) State 5 (buck).

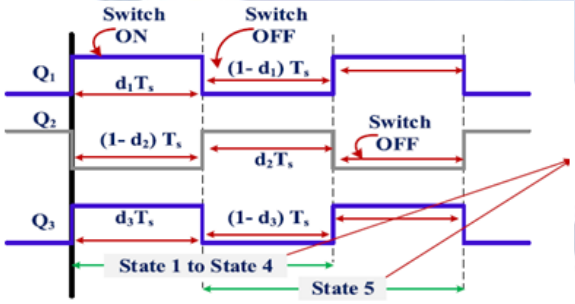

Fig. 4 State of operation of proposed FPC.

D. Third State: SIDO Converter (Battery-to-AC) Power transfer Status

The energy stored in the battery has been transferred to the load. As the battery empties, the current through the inductor iL2 grows linearly from zero to d3Ts. Between d3Ts and Ts, the iL2 current exhibits a negative slope. Whether or not the switch is engaged, Q3 boosts output at the gearbox and drives. Since Q1 is not necessary for the transfer of power from the battery to the load, it is constantly in the OFF state. The voltage drop across the load when discharging a battery looks like this:

$$V_0 = \frac{1}{1-d_3} V_{bat} \quad (6)$$

$$V_{01} = \frac{1}{1-d_3} V_{bat} \quad (7)$$

E. Condition 4: DIDO (Dual Input Dual Output) Converter Power Status (PV/Battery Power Indicator)

The battery and PV might be used to meet the high power needs of EVs. The currents in the inductor, iL1 and iL2, rise linearly from 0 to d1Ts when the gates of switches Q1 and Q3 are closed. The free gate signal is now being sent to Q2. The currents via inductors iL1 and iL2 decrease precipitously (negative slope) when switches Q1, Q3 are closed. Therefore, electricity from both the battery and the solar panels is sent to the load through diodes D1 and D2. Using Eqs.(8-9) we can get the total output voltage from both generators:

$$V_0 = \frac{1}{1-d_1} V_{PV}, (or) V_0 = \frac{1}{1-d_3} V_{bat} \quad (8)$$

$$V_{01} = \frac{1}{1-d_1} V_{PV}, (or) V_{01} = \frac{1}{1-d_3} V_{bat} \quad (9)$$

F. Converter State 5 (Power Transfer from Load to Battery): SIDO.

The battery benefits from the drive train's conserved kinetic energy thanks to regenerative braking. The following is the progression from this condition to the next: In this configuration, Q1 is always turned off, but Q2, Q3, and Q4 are always active. In combination with Q3, the on-off cycle of Q2 charges the battery.

$$V_{bat} = d_2 V_O \quad (10)$$

The second output in the same condition is used to charge the battery via regenerative braking. Here's how we get to the control relation:

$$V_{01} = d_3 V_O \quad (11)$$

3. Control Strategy

The 12V, 7Ah battery serves as the energy storage unit, while the 100 W photovoltaic (PV) panel serves as the primary source (it is composed of two 50 W Mono crystalline PV panels). By hooking up the PV panel to a regular P&O MMPT controller, the MPP may be

calculated. For demonstration purposes, we build a scaled-down prototype of the proposed converter and test it in a range of operational modes and input/output voltage arrangements. Controlled switches in the power circuit are MOSFETs (IRFP250N), whereas the uncontrolled ones are diodes (UF5408). As shown in Figure 6, the ANN controller (dsPIC30F2010) implements a switch and state selection control algorithm. In Fig.5 and Fig.6, the advanced ANN controller determines the duty cycles for MOSFETs Q1, Q2, and Q3. The duty cycles for Q1, Q2, and Q3 are shown in Fig.6(b). By comparing the reference output voltages to the actual load output voltages (Vo and V01), an error signal is generated that may be used to calculate the current references (IL1ref and IL2ref). To choose the best ANN controller, we utilise the auto-turning tool in MATLAB and then implement it in the dsPIC30F2010 controller. Q1, Q2 duty cycles are utilised as standards, and adjustments are made based on the present inaccuracy. By comparing the 10 kHz triangle carrier signal to a reference signal, the duty cycles Q1, Q2 may be determined. At the same time that Q2 is being toggled in the opposite manner, Q1 and Q3 are being toggled on and off with the same duty cycle. As a consequence, the NOT gate is used to generate duty cycles for Q2.

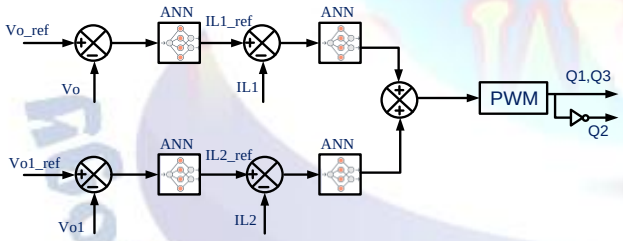

Fig.5 PWM generator with proposed ANN control

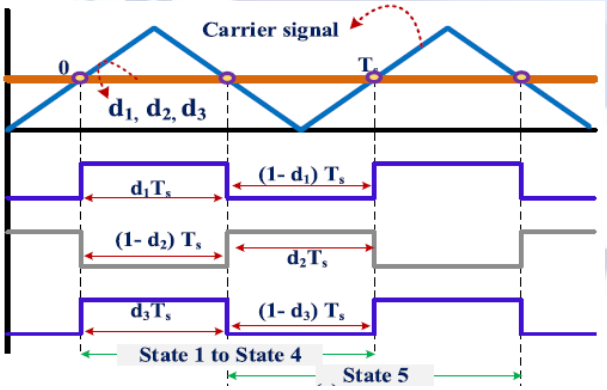

Fig.6 duty cycle of proposed ANN FPC converter control

4. ANN CONTROLLER

Use Improvements in efficiency, minimum ripple in torque and flux, better driving range, and decreased battery depletion rate are all instantly noticeable when AI is employed to govern the motors that move electric cars. Classical approaches like Ziegler-Nichols tuning have been embraced alongside more recent, artificial intelligence (AI)-based methods like fuzzy logic, ANNs, ANFIS (adaptive neural fuzzy inference systems), GAs (genetic algorithms), and PSOs (particle swarm optimisation). In this research, we solely investigate tuning techniques based on adaptive neural networks, since we want to find the optimal values for the torque controller's parameters. Due to its simple structural design, robustness against parameter changes, and ability to approximate complex nonlinear functions, adaptive neural networks are well suited for use in an eCAR control system. Researchers have used ANNs with DTC techniques in a variety of settings, including speed estimation for motors, state estimation, the construction of speed and torque controllers, and vector selection algorithms. There are a wide variety of neural networks available today [30], including feed forward multilayer neural networks and recursive neural networks. A basic ANN block design is seen in Figure 7.

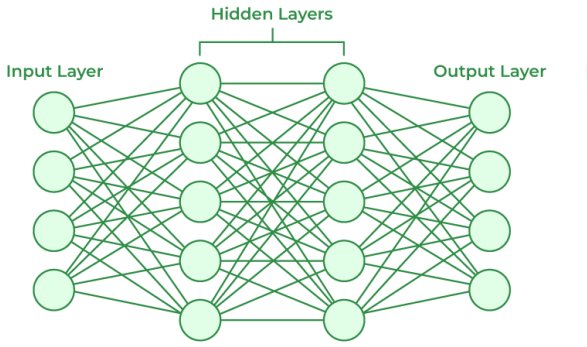

Fig. 7 Block Diagram of ANN Block

In this article, an adaptive neural network based torque controller for the inner current loop is developed to reduce the capacitor voltage error and boost the efficiency of the propulsion motor (see Figure 8). In its stead, the ANN-tuned torque controller is presented as an alternative to the standard controller. With an input layer of two neurons, a hidden layer of one hundred, and an output layer of only one, the ANN controller we developed has a 1, 100, 1 architecture. the ANN's steady-state error output is used as an input to the PI controller, which then uses that value to set the voltage of the reference dc capacitor. An artificial neural network (ANN) structure with two inputs, a hidden layer, and a

single output is shown in MATLAB Simulink (Figure 8).

Dc capacitor error data ('Vo') and dc capacitor error delta data ('D_Vo') are utilised to sample network inputs. The ANN's settings. The network's output is used to fine-tune the torque controller via an iterative application of the Levenberg Marquardt optimisation algorithm [31,32], with the input and hidden layers each representing a hyperbolic tangent sigmoid transfer function and the output layer representing a pure line transfer function. Iterations of the ANN algorithm consist of:

Step 1: The network is first fed inputs consisting of both the initial torque error and the subsequent change in torque error. With two inputs, the vector matrix [X] is represented as [X] 2 _ 1.

Step 2: The network's desired variables are then used to guide the selection of targets. The one-output target vector matrix is denoted by [t] 1 _ 1.

Step 3: Levenberg-Marquardt optimisation technique is then used to init and adjust the weights and biases. The output vector matrix, y, is equal to the product of the row matrices of the weights and biases, [w] and [b].

Step 4: With the objective parameter set to a minimum, the ANN is trained using the information from Steps 1 and 2. When the error data, represented as an error vector matrix (E), indicates that the training has converged to the stated objective parameters or epochs, the training process is terminated.

$$E = \frac{\sum_{i=1}^{n}(t_i - y_i)^2}{I} \qquad (12)$$

Where n is the total number of outputs, I is the number of iterations, and E is the error data matrix produced using a mean squared error as the objective function.

Step 5: Following optimisation during network training, the steady-state error at its optimised value is returned as the final output.

Step 6: The PI controller takes its input from the optimised steady-state error signal to generate a dc voltage at the capacitor.

The neural network's input, output, goal, and error data are all calculated based on the simulated step input generated by the whole vehicle model. By setting the bias to 1, then adding the values and updated weights, the torque error is minimized [33]. At the 14th epoch, the optimum choice is the number 1.0155× (10^{-7}) because it is closest to zero. Simply enter "nntool" at the MATLAB prompt to begin the network creation process. Figure 8 shows the "genism (network)" command being used to develop the Simulink model.

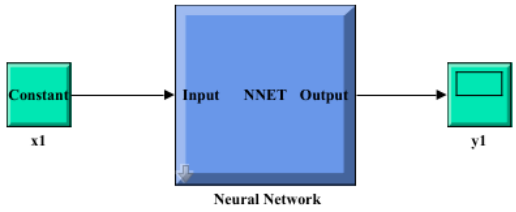

Figure 8. Simulink model of an ANN.

5. Results and Discussion

G. Steady state characteristics of proposed four-port converter (FPC)

Because The performance curve of the system and the results of a MATLAB/Simulink 2016a simulation are shown in Figure 9. Figure 9 depicts the SPV array in steady state operation. Maximum dc voltage for an ANN-based capacitor is shown in Figure 5 to be 62 V, while maximum dc current for an ANN-based inductor is shown to be 5 A. Using the proposed cutting-edge ANN controller, we were also able to measure maximum solar power of 21V and 8A. The boost converter is shown in action with a 5 A inductor current and a 62 V motor capacitor voltage and Vo1 in Figure 9. The electric vehicle shown in Fig. 1 requires the IM motor to operate at its maximum rated speed (N) and electromagnetic torque (Te) in order to go forward. When there is a rippling current at the VSI's DC connection, Te will fluctuate somewhat. A smooth start may be seen in the speed-time characteristics of a starting IM motor. The battery is in a charging condition when solar intensity is highest (Ib).

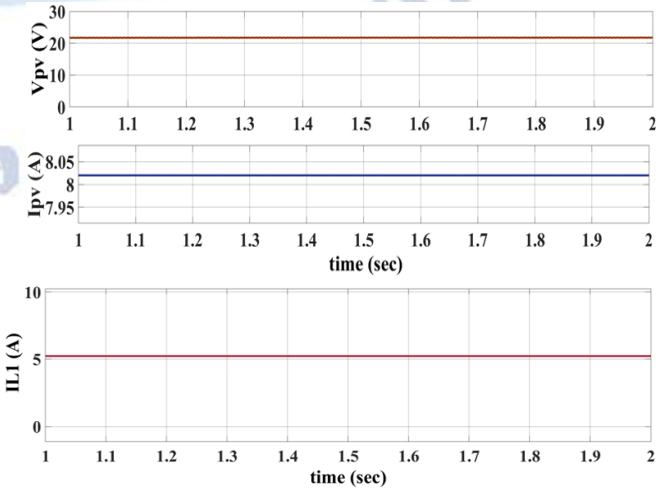

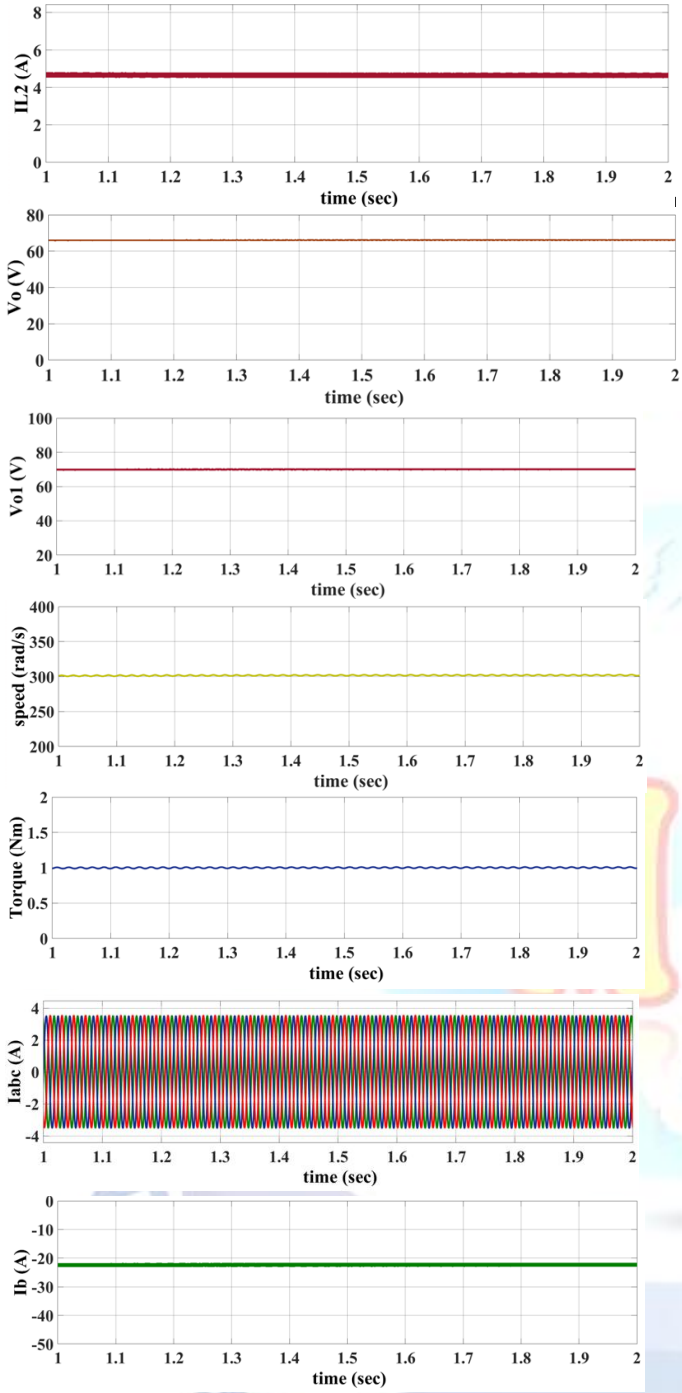

Fig .9 Steady state condition of proposed four-port converter (FPC)

H. Dynamic Characteristics of proposed four-port converter (FPC)

Figure 10 shows the SPVWPS's dynamic properties. The solar irradiance is dynamically changed from a peak of 1000 W/m2 at zero seconds to a minimum of 200 W/m2 at one minute and seventy-five hundredths of a second and a peak of 800 W/m2 at two minutes and twenty-five thousandths of a second. Figure 8 demonstrates that the proposed ANN controller can quickly monitor maximum power despite the unpredictable nature of variations in solar irradiation. In Fig.10, the inductor current fluctuates with the intensity of the sunlight while Vo and Vo1 are maintained constant at 62 V. The quantity of sunshine is like solar irradiance in that it impacts the charging and discharging current of a battery energy storage system. The solar panel's battery charger activates when solar radiation is high and turns off when it is weak. Fig. 10 depicts how the intensity of solar radiation has an effect on the IM motor's speed (N), electromagnetic torque (T), pump torque (T), and phase a stator current (Iabc). As was seen, the IM motor quickly reaches its steady-state value. An electric vehicle's electromagnetic torque, which indicates the motor's steady performance throughout a wide range of light levels, cancels out the torque generated by the vehicle's load.

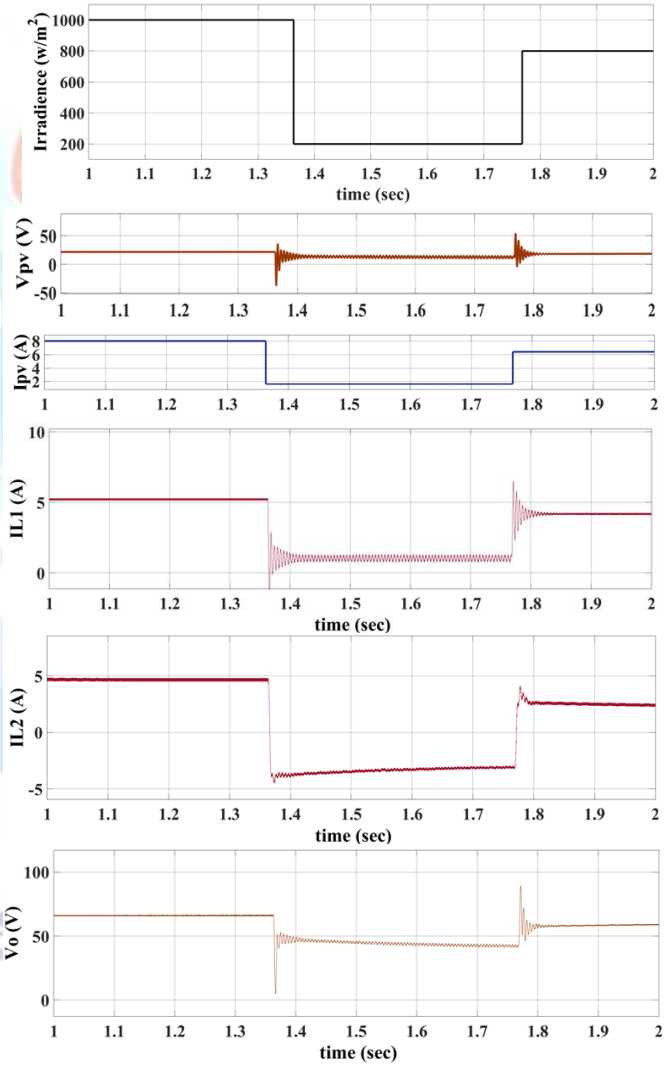

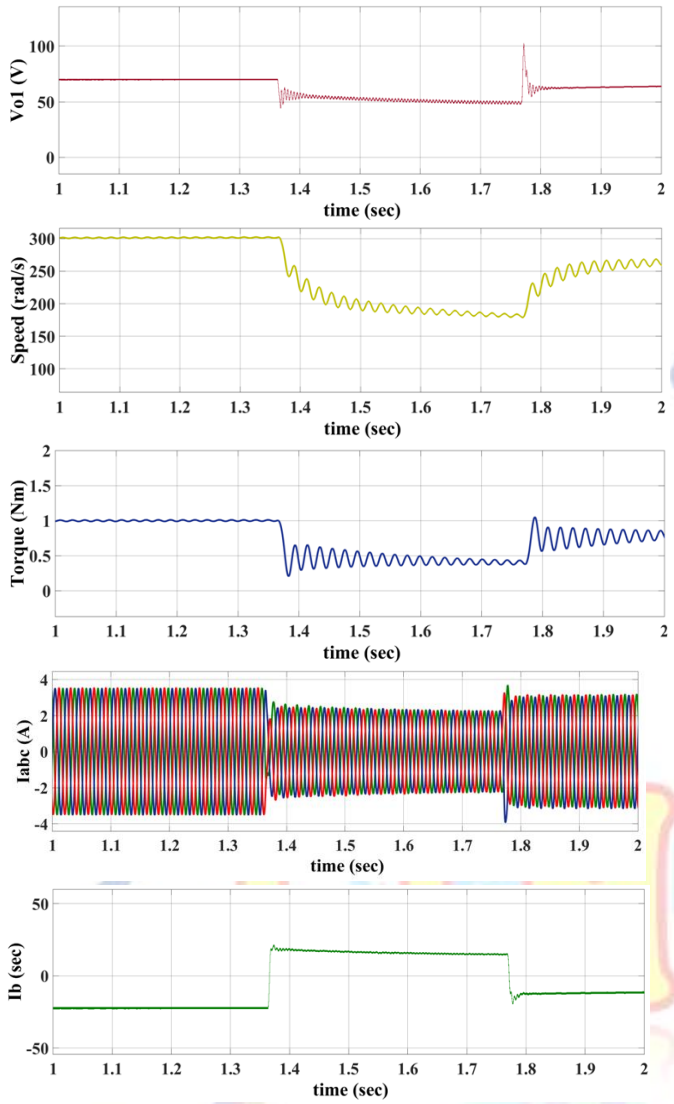

Fig .10 Dynamic condition of proposed four-port converter (FPC)

6. Conclusion

In conclusion, this paper has presented a modified non-isolated four-port converter (FPC) designed for electric vehicle (EV) applications, emphasizing its capability to efficiently accommodate energy resources with varying voltage and current characteristics. The FPC offers simultaneous buck and boost output capabilities, making it a versatile and adaptable solution for diverse EV subsystems. The key advantages of the proposed FPC include a reduced component count, simplified control strategy, and bidirectional power flow functionality, which enhances its reliability and cost-effectiveness. Moreover, the converter is well-suited for harnessing regenerative energy during braking, contributing to the overall energy efficiency of the EV. The steady-state and dynamic behavior of the converter were analyzed, and a control scheme was presented to regulate power flow between different energy sources. Additionally, a small-signal model was developed to facilitate the converter's design process. To validate the design and assess its performance, extensive simulations and experimental tests were conducted using MATLAB. These results demonstrated the converter's ability to meet the power conversion requirements of electric vehicles across various operating conditions. Furthermore, the integration of an Advanced Controller (ANN) was proposed to enhance the converter's adaptability and intelligence, allowing for real-time optimization of power flow and improved performance in dynamic EV environments. In conclusion, the modified four-port converter presented in this paper offers a promising solution for enhancing the efficiency and performance of electric vehicles. Its ability to accommodate diverse energy resources, coupled with its bidirectional power flow capability and potential integration with an ANN controller, positions it as a valuable contribution to the evolving landscape of electric vehicle power electronics. Future work may involve further optimization, validation, and practical implementation of this converter in real-world EV applications.

Conflict of interest statement

Authors declare that they do not have any conflict of interest.

References

[1] H. Wu, Y. Xing, Y. Xia, and K. Sun, ``A family of non-isolated three-port converters for stand-alone renewable power system,'' IEEE Trans. Power Electron., vol. 1, no. 11, pp. 1030_1035, 2011.

[2] K. I. Hwu, K.W. Huang, andW. C. Tu, ``Step-up converter combining KY and buck-boost converters,'' Electron. Lett., vol. 47, no. 12, pp. 722_724, Jun. 2011.

[3] H. Xiao and S. Xie, ``Interleaving double-switch buck_boost converter,'' IET Power Electron., vol. 5, no. 6, pp. 899_908, Jul. 2012.

[4] H. Kang and H. Cha, ``A new nonisolated High-Voltage-Gain boost con- verter with inherent output voltage balancing,'' IEEE Trans. Ind. Electron., vol. 65, no. 3, pp. 2189_2198, Mar. 2018.

[5] T. Bang and J.-W. Park, ``Development of a ZVT-PWM buck cascaded buck_boost PFC converter of 2 kW with the

widest range of input voltage," IEEE Trans. Ind. Electron., vol. 65, no. 3, pp. 2090_2099, Mar. 2018.

[6] C.-C. Lin, L.-S. Yang, and G. W. Wu, ``Study of a non-isolated bidirectional DC_DC converter," IET Power Electron., vol. 6, no. 1, pp. 30_37, Jan. 2013.

[7] M. A. Khan, A. Ahmed, I. Husain,Y. Sozer, and M. Badawy, ``Performance analysis of bidirectional DC_DC converters for electric vehicles," IEEE Trans. Ind. Appl., vol. 51, no. 4, pp. 3442_3452, Jul. 2015.

[8] S. Dusmez, A. Khaligh, and A. Hasanzadeh, ``A zero-voltage-transition bidirectional DC/DC converter," IEEE Trans. Ind. Electron., vol. 62, no. 5, pp. 3152_3162, May 2015.

[9] H. Zhu, D. Zhang, B. Zhang, and Z. Zhou, ``A nonisolated three-port DC_DC converter and three-domain control method for PV-battery power systems," IEEE Trans. Ind. Electron., vol. 62, no. 8, pp. 4937_4947, Aug. 2015.

[10] M. B. Camara, H. Gualous, F. Gustin, and A. Berthon, ``Design and new control of DC/DC converters to share energy between supercapacitors and batteries in hybrid vehicles," IEEE Trans. Veh. Technol., vol. 57, no. 5, pp. 2721_2735, Sep. 2008.

[11] T. Kim and S. Kwak, ``Single pole switch leg based multi-port converter with an energy storage," IET Power Electron., vol. 9, no. 6, pp. 1322_1330, May 2016.

[12] H. Wu, Y. Lu, L. Chen, P. Xu, X. Xiao, and Y. Xing, ``High step-up/step down non-isolated BDC with built-in DC-transformer for energy storage systems," IET Power Electron., vol. 9, no. 13, pp. 2571_2579, Oct. 2016.

[13] A. Ajami, H. Ardi, and A. Farakhor, ``Design, analysis and implementation of a buck-boost DC_DC converter," IET Power Electron., vol. 7, no. 7, pp. 1906_1914, Nov. 2014.

[14] M. R. Banaei, H. Ardi, and A. Farakhor, ``Analysis and implementation of a new single switch buck-boost DC_DC converter," IET Power Electron., vol. 7, no. 12, pp. 2902_2913, May 2014.

[15] E. Babaei and O. Abbasi, ``Structure for multi-input multi-output DC_DC boost converter," IET Power Electron., vol. 9, no. 1, pp. 9_19, Jan. 2016.

[16] A. Nahavandi, M. T. Hagh, M. B. B. Shari_an, and S. Danyali, ``A non isolated multiinput multioutput DC_DC boost converter for electric vehicle applications," IEEE Trans. Power Electron., vol. 30, no. 4, pp. 1818_1835, Apr. 2015.

[17] M. R. Banaei, H. Ardi, R. Alizadeh, and A. Farakhor, ``Non-isolated multi input single-output DC/DC converter for photovoltaic power generation systems," IET Power Electron., vol. 7, no. 11, pp. 2806_2816, Nov. 2014.

[18] F. Akar, Y. Tavlasoglu, E. Ugur, B. Vural, and I. Aksoy, ``A bidirectional nonisolated multi-input DC_DC converter for hybrid energy storage sys- tems in electric vehicles," IEEE Trans. Veh. Technol., vol. 65, no. 10, pp. 7944_7955, Oct. 2016.

[19] Y. Yuan-Mao and K. W. E. Cheng, ``Multi-input voltage-summation con- verter based on switched-capacitor," IET Power Electron., vol. 6, no. 9, pp. 1909_1916, Nov. 2013.

[20] Y. Ye and K. W. E. Cheng, ``Multi-port voltage-subtracting circuit based on resonant switched-capacitor," IET Power Electron., vol. 5, no. 6, pp. 693_701, Jul. 2012.

[21] Y. Ye and K. W. E. Cheng, ``Single-switch single-inductor multi- output pulse width modulation converters based on optimised switched- capacitor," IET Power Electron., vol. 8, no. 11, pp. 2168_2175, Nov. 2015.

[22] H. Behjati and A. Davoudi, ``Single-stage multi-port DC_DC converter topology," IET Power Electron., vol. 6, no. 2, pp. 392_403, Feb. 2013.

[23] D. Gunasekaran and L. Umanand, ``Integrated magnetics based multi-port bidirectional DC_DC converter topology for discontinuous-mode operation," IET Power Electron., vol. 5, no. 7, pp. 935_944, Aug. 2012.

[24] H. Tao, A. Kotsopoulos, J. L. Duarte, and M. A. M. Hendrix, ``Family of multiport bidirectional DC_DC converters," IEE Proc.-Electr. Power Appl., vol. 153, no. 3, pp. 451_458, May 2006.

[25] O. C. Onar, J. Kobayashi, and A. Khaligh, ``A fully directional universal power electronic interface for EV, HEV, and PHEV applications," IEEE Trans. Power Electron., vol. 28, no. 12, pp. 5489_5498, Dec. 2013.

[26] T. K. Santhosh and C. Govindaraju, ``Dual input dual output power converter with one-step-ahead control for hybrid electric vehicle applications," IET Electr. Syst. Transp., vol. 7, no. 3, pp. 190_200, Sep. 2017.

[27] C. Duan, C. Wang, Z. Li, J. Chen, S. Wang, A. Snyder, and C. Jiang, ``A solar power-assisted battery balancing system for electric vehicles," IEEE Trans. Transport. Electri_c., vol. 4, no. 2, pp. 432_443, Jun. 2018.

[28] F. Akar, Y. Tavlasoglu, and B. Vural, ``An energy management strategy for a concept battery/ultracapacitor electric vehicle with improved battery life," IEEE Trans. Transport. Electri_c., vol. 3, no. 1, pp. 191_200,Mar. 2017.

[29] D. A. Savio, V. A. Juliet, B. Chokkalingam, S. Padmanaban, J. B. Holm-Nielsen, and F. Blaabjerg, ``Photovoltaic integrated hybrid microgrid structured electric vehicle charging station and its energy management approach," Energies, vol. 12, no. 1, p. 168, Jan. 2019.

[30] Tummala, S.K.; Dhasharatha, G. Artificial Neural Networks based SPWM technique for speed control of Permanent Magnet Synchronous Motor. In Proceedings of the E3S Web of Conferences, SeFet 2019: 1st International Conference on Sustainable Energy and Future Electric Transportation, Gokaraju Rangaraju Institute of

Engineering & Technology, Hyderabad, India, 14–16 February 2019; Volume 87, p. 01030.

[31] Jia, Z.; Kim, B. Direct Torque Control with Adaptive PI Speed Controller based on Neural Network for PMSM Drives. In Proceedings of the MATECWeb Conferences, International Conference on Electrical Engineering, Control and Robotics (EECR 2018), Chengdu, China, 12–14 January 2018; Volume 160, p. 02011.

[32] Rao, V.M.V.; Kumar, A.A. Artificial Neural Network and Adaptive Neuro Fuzzy Control of Direct Torque Control of Induction Motor for Speed and Torque Ripple Control. In Proceedings of the 2018 2nd International Conference on Trends in Electronics and Informatics (ICOEI), Tirunelveli, India, 11–12 May 2018; pp. 1416–1422.

[33] Djeriri, Y.; Meroufel, A.; Massoum, A. Artificial neural network based direct torque control of doubly fed induction generator. J. Electr. Eng. 2014, 14, 71–79